Journal of Catalysis **204,** 35–52 (2001)
doi:10.1006/jcat.2001.3369, available online at http://www.idealibrary.com on IDEAL®

Island Formation during Kinetic Rate Oscillations in the Oxidation of CO over Pt/SiO_2: A Transient Fourier Transform Infrared Spectrometry Study

Paul T. Fanson, W. Nicholas Delgass, and Jochen Lauterbach[1]

School of Chemical Engineering, Purdue University, West Lafayette, Indiana 47907-1283

Received January 29, 2001; accepted August 1, 2001

Transient Fourier transform infrared spectroscopy (FTIR) spectroscopy and mass spectroscopy were used in tandem to study CO adsorption and kinetic rate oscillations in the oxidation of CO at intermediate pressure (1–10 Torr) on a series of silica gel-supported platinum catalysts of varying dispersion and preparation. FTIR shows that the stretching frequency of linearly bonded CO decreases as the dispersion of the platinum particles increases (2076 cm^{-1} for $D = 25\%$ to 2058 cm^{-1} for $D = 99\%$), but CO bonded to electron-deficient platinum (CO–$Pt^{\delta+}$) results in a frequency of $\sim$2080 cm^{-1} for all particle sizes. Isotope-mixing experiments and dipole coupling simulations were performed in order to determine the dipole and chemical components of the coverage-dependent IR peak shift on supported platinum. The results compare favorably to single-crystal studies and show a chemical shift of 10 cm^{-1} and a dipole shift of 25 cm^{-1} that are independent of particle dispersion. Reaction studies at $T = 180$–$300^{\circ}C$ and $O_2 : CO = 0.5$–4.0 suggest that the oxidation/reduction model and the carbon deposition model cited in the literature are both inadequate to explain the observed oscillations over these catalysts. A mechanism is suggested in which densely packed islands of CO block a portion of the active sites during the reaction. Differences in catalyst precursor (chloroplatinic acid or tetraammine platinum(II) nitrate) affect the amplitude of the oscillations observed in this study. The feedback mechanism driving the oscillations remains unclear but is most likely related to the Pt(100) or Pt(110) surface-phase transition or chlorine impurities supporting the formation of islands through electrostatic interaction.

Key Words: **CO oxidation; transient FTIR; rate oscillations; Pt/SiO_2; island formation; dipole coupling.**

1. INTRODUCTION

The oxidation of carbon monoxide is one of the most intensely studied reactions in the history of catalysis. In particular, the reaction over platinum has received a great deal of attention. The importance of CO oxidation in pollution control and automotive catalysis, the simple nature of the reactants, and the utility of CO as a probe molecule have made the study of CO oxidation both industrially relevant and fairly straightforward. However, there are aspects of the reaction mechanism that remain unexplained.

Self-sustained kinetic oscillations have been reported over both supported catalysts and single crystals for decades (1–16). The mechanism behind oscillations on Pt(100) and Pt(110) single crystals under ultrahigh vacuum conditions has been explained as being driven by surface-phase transitions that alter the adsorption properties of both oxygen and carbon monoxide (3, 7, 17). The mechanism that occurs on supported catalysts, however, has not been adequately explained.

The two most commonly cited models proposed for oscillations over supported catalysts are the carbon model (18) and the oxidation/reduction model (19). Both models suggest a slow poisoning of the active sites followed by a subsequent cleaning and regeneration of activity. The carbon model proposes that a carbonaceous deposit poisons active sites, while the oxidation/reduction model suggests that an oxidized form of platinum blocks sites. Both models generally predict oscillations with a period of several minutes during which the surface coverage of CO cycles between 0 and 100%. Although no solid experimental evidence exists to support the carbon model, some groups have observed an IR absorption peak at 2120 cm^{-1} which has been observed to oscillate during the reaction over a Pt/Al_2O_3 catalyst at both atmospheric (14) and reduced pressure (1–10 Torr) (15). The peak at 2120 cm^{-1} is associated with oxidized platinum (15, 20), and the authors offer this peak as proof of the oxidation/reduction model. Additional X-ray diffraction experiments at atmospheric pressure (21) over Pt/SiO_2 also support the oxidation/reduction model.

Other authors, however, either have not observed a peak at 2120 cm^{-1} at all (1, 12) or have not observed the peak to oscillate (8, 9, 16). In the latter case, the absorption peak at $\sim$2070 cm^{-1} (linearly bonded CO on reduced Pt) is the only peak exhibiting oscillatory behavior. In general, the oscillations observed in these studies tend to have much shorter periods than the experiments in which the oscillatory 2120-cm^{-1} peak was observed. More recent modeling attempts have also shown that the oxidation/reduction model is not completely consistent with transient experiments

[1] To whom correspondence should be addressed. Fax: (765) 494-0805. E-mail: jochen@ecn.purdue.edu.

0021-9517/01 $35.00

performed over supported platinum catalysts (16, 22). Thus the oxidation/reduction model does not seem to apply to all supported platinum catalysts under all conditions.

An additional model that has not received as much attention is the CO island formation model. The model was first suggested as a way to explain observations made using infrared spectroscopy that show a constant CO stretching frequency over a wide range of coverage on the surface of the supported catalyst under reaction conditions (23–25). The observed frequency was within a few wavenumbers of the value obtained for a complete monolayer of CO. It is known that the infrared spectrum of CO adsorbed on platinum typically exhibits a coverage-dependent frequency shift of $\sim$30 cm^{-1} (26, 27). This frequency shift is in part a consequence of increasing dipole–dipole interactions as the surface saturates with CO (28–30). Thus, the dipole–dipole interaction experienced by surface CO under reaction conditions is similar to the interaction at saturation. It is therefore likely that CO exists in the form of closely packed islands on the catalyst surface, thus creating a local environment similar to that at saturation.

Infrared studies on platinum single crystals have also suggested the existence of CO islands (31, 32). In addition, imaging techniques such as PEEM, EMSI, and FEM have also confirmed the existence of CO and oxygen islands on the surfaces of both single-crystals (9, 33–35) and 100-Å platinum particles (11). One group (1, 13) has suggested a mechanism to explain the oscillations in which islands of CO periodically nucleate, grow, and are eventually consumed by surface oxygen. Modeling attempts (36) have shown that the existence of islands can account for the general shape of oscillations observed on certain catalysts, namely, the short-period oscillations observed in the absence of the 2120-cm^{-1} absorption peak.

In this study we have examined oscillations in the oxidation of CO and oxygen over silica-supported platinum with the goal of determining the mechanism responsible for the nonlinear behavior. In addition, we have performed isotope-mixing experiments in order to resolve the dipole and chemical components of the coverage-dependent peak shift of CO adsorbed on supported platinum. We employed transient Fourier transform infrared spectroscopy (FTIR) to monitor CO on the surface of the catalyst and used mass spectrometry (MS) to analyze the gas-phase reaction products. Catalysts with a wide range of metal loadings and particle dispersions were compared with respect to the adsorption and desorption of CO and the behavior of the catalyst in the oscillatory regime of the reaction.

2. EXPERIMENTAL METHODS

A series of silica-supported platinum catalysts was synthesized using incipient wetness impregnation. In all cases, the silica used was a 130- to 270-mesh column chromatography silica gel (Aldrich, 28860-8, 500 m^2/g, average pore diameter = 60 Å). A portion of the catalysts was synthesized using chloroplatinic acid (Aldrich) as a precursor, while the remaining samples were synthesized using tetraammine platinum(II) nitrate (Strem). Catalysts made from these two precursors are referred to as the chloroplatinic acid catalysts and the amine–nitrate catalysts, respectively. Once the impregnation was complete, the samples were dried overnight in air at 110°C. The catalysts were then calcined in a mixture of 20% oxygen in helium with a temperature program that increased linearly from room temperature to 300°C over 2 h and then held at 300°C for 6 h. The gas was switched to pure helium, and the temperature was decreased linearly from 300 to 200°C over 1 h. The catalysts were then reduced in 20% hydrogen in helium for 12 h at 200°C. In addition, a portion of the highest loading amine–nitrate catalyst was postimpregnated with 0.044 M HCl in order to study the effect of chlorine impurities.

The metal loading of each sample was measured using atomic absorption (Perkin–Elmer Atomic Absorption Spectrometer 3110), and the dispersion of each sample was determined from CO chemisorption (Micromeritics ASAP 2000). Transmission electron microscopy (TEM) was performed on each sample to confirm the particle sizes obtained from the chemisorption measurements. The resulting catalyst properties are summarized in Table 1.

For each experiment, 25–30 mg of catalyst was pressed under 4000 psig into an IR transparent wafer approximately 0.2 mm thick and 14 mm in diameter. The wafer was then placed into a sample holder as described previously (9). The sample holder was placed inside a 2.75-in. conflat five-way cross equipped with two CaF_2 windows. The reactor was kept at a base pressure of 10^{-9} Torr by an 80 L/s turbomolecular pump backed by a rotary vane mechanical pump (Alcatel). A gate valve located just above the turbomolecular pump allowed the conductance of the vacuum system to be varied so that the pressure in the reactor could be adjusted between 10^{-9} Torr and atmospheric pressure. The pressure inside the reactor was monitored with a cold

TABLE 1

Summary of Prepared Catalysts

Catalyst ID	Precursor	Loading (wt%)	Dispersion[a]	d (nm)[b]
0.05-Pt/SiO_2–NO	$Pt(NH_3)_4(NO_3)_2$	0.05	99%	1.7
0.6-Pt/SiO_2–NO	$Pt(NH_3)_4(NO_3)_2$	0.6	90%	1.8
3.0-Pt/SiO_2–NO	$Pt(NH_3)_4(NO_3)_2$	3.0	60%	2.8
1.0-Pt/SiO_2–Cl	H_2PtCl_6	1.0	—[c]	—
3.1-Pt/SiO_2–Cl	H_2PtCl_6	3.1	25%	6.7

[a] From CO chemisorption assuming 1 : 1 Pt : CO stoichiometry.

[b] Average particle diameter based on dispersion and assuming hemispherical shape.

[c] Not measured due to lack of sample.

cathode gauge (Varian) for pressures below 1 mTorr and a convecTorr gauge (Varian) for pressures between 1 mTorr and 1 atm. Six mass flow controllers (Brooks, 0–50 ml/min) were used to meter gas flow. All gases used in this study were research grade.

The reactor was connected to a mass spectrometer (Hiden HAL 201RC) via a variable conductance leak valve (Varian). The mass spectrometer was kept at a base pressure of 10^{-9} Torr by a 70 L/s turbomolecular pump backed by a rotary vane mechanical pump (Varian), has a range of 1–200 amu, and is capable of sampling 100 data points per second in multi-ion detection (MID) mode. In this study, three gases (CO, O_2, and CO_2) were typically monitored at a rate of 15 data points per second.

Surface species were monitored via a Nicolet Protégé 460 FTIR spectrometer. The spectrometer was equipped with a nitrogen-cooled MCT detector with a range of 650–4000 cm^{-1}. Excellent signal to noise could typically be achieved with eight scans at 2 cm^{-1} resolution. All spectra were referenced to a background scan of the catalyst under vacuum at the temperature of the experiment, except in the case of thermal desorption experiments where the background was taken at room temperature. The spectrometer is capable of taking two to three spectra per second.

3. RESULTS AND DISCUSSION

3.1. CO Adsorption

For CO adsorption experiments, two different catalyst pretreatments were used. For the first pretreatment, referred to as the reducing pretreatment, the catalyst was heated in vacuum to 200°C, reduced in flowing H_2 for 30 min at a pressure of 10 mTorr, evacuated, and heated to 300°C. The catalyst was held at this temperature and oxidized for 30 min at a pressure of 10 mTorr of O_2. The sample was then briefly evacuated at 300°C, and the gas was switched back to H_2. The catalyst was allowed to cool in H_2 to room temperature, at which time the CO adsorption experiments were performed. The second pretreatment, referred to as the oxidizing pretreatment, was identical to the first, except that the final reduction step was omitted, and the catalyst was allowed to cool to room temperature in vacuum.

Once the system reached room temperature, CO was passed over the catalyst at a pressure of 10 mTorr. At this pressure, the catalyst saturated with CO in less than a second. Saturation was reached when the integrated area of the IR absorption peak for linearly bonded CO remained constant over time. Dosing the catalyst with lower pressures of CO (1×10^{-8} to 1×10^{-5} Torr) resulted in slower growth to saturation. The frequency and shape of the absorption peak were unchanged during the adsorption. This phenomenon has been observed previously (37, 38) and is due to the high rate of CO adsorption compared to the rate of diffusion into the catalyst pellet. Because the sticking coefficient of CO is of order 1 (31) and there is virtually no desorption at temperatures below 200°C (31, 39), the pellet saturates with CO in a chromatographic manner. Each platinum particle becomes fully saturated as the CO front moves into the wafer.

TABLE 2

Summary of Peak Position and Full Widths at Half-Maximum (FWHM) for Linearly Bonded CO after the Oxidizing and Reducing Pretreatments

	Oxidized		Reduced	
Catalyst ID	Peak position (cm^{-1})	FWHM (cm^{-1})	Peak position (cm^{-1})	FWHM (cm^{-1})
0.05-Pt/SiO_2–NO	2083	37	2058	52
0.6-Pt/SiO_2–NO	2082	21	2065	46
3.0-Pt/SiO_2–NO	2086	20	2076	34
1.0-Pt/SiO_2–Cl	2077	30	2067	32
3.1-Pt/SiO_2–Cl	2092	25	2072	32

Figures 1 and 2 compare the IR absorption spectra observed after room temperature saturation with CO following the reducing and oxidizing pretreatment. The figures also compare the absorption peaks that are observed for the chloroplatinic acid and amine–nitrate catalysts. Table 2 summarizes the peak positions and full widths at half-maximum (FWHM) for each peak shown in Figs. 1 and 2. Several differences in the four spectra are apparent. First, each spectrum shows an intense, sharp peak in the 2050–2100 cm^{-1}region of the spectrum, which is assigned to linearly bonded CO on platinum (40). In addition, bridge-bonded CO is evident from the broad peaks below 1900 cm^{-1}. In all catalysts studied, the reducing pretreatment resulted in a larger bridge-bonding peak than did the oxidizing pretreatment. Bridge bonding on supported platinum is typically observed at ~1850 cm^{-1} (40), which is consistent with the catalyst that underwent the oxidizing pretreatment. However, the reducing pretreatment resulted in a broad band about 1770 cm^{-1}. A stretching frequency this low is fairly rare and is typically assigned to threefold bonding sites (41–43), although a more highly coordinated fourfold bonding site is also possible.

The main differences in the spectra shown in Figs. 1 and 2 lie in the linearly bonded CO region. In all five catalysts, the reducing pretreatment resulted in a broader peak than did the oxidizing pretreatment. On average, the FWHM increases by ~50% (27 to 39 cm^{-1}) and the increases in width are more pronounced in the amine–nitrate samples. Additionally, the peaks resulting from the oxidized catalysts are more symmetric, especially the samples prepared from the amine–nitrate precursor. The peaks from the reduced catalysts, however, show low-frequency inhomogeneous line broadening in addition to a distinct high-frequency shoulder. Infrared absorption peaks with a similar shape were investigated by Greenler and co-workers (38, 44). They

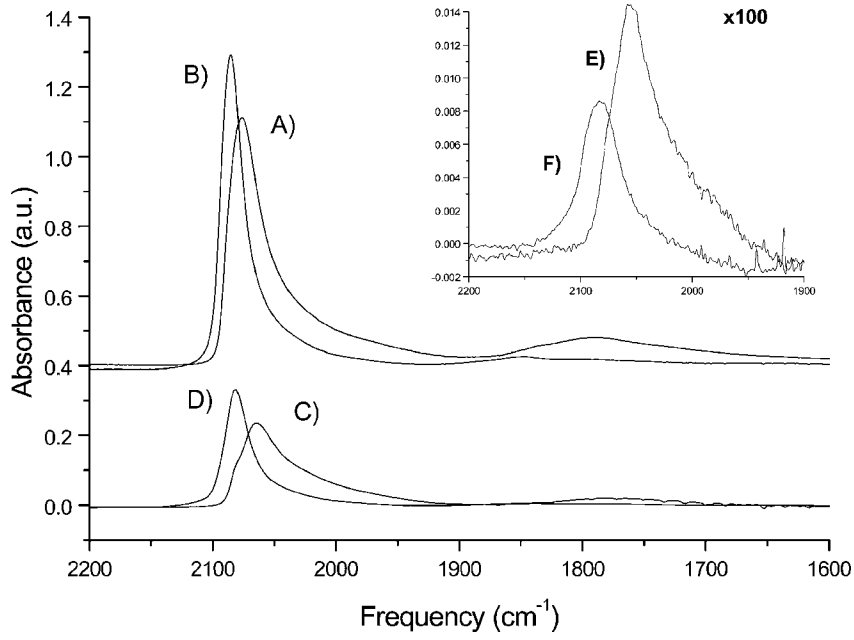

FIG. 1. Infrared spectra of CO adsorbed onto reduced and oxidized Pt/SiO_2 catalysts prepared from tetraammine platinum(II) nitrate at room temperature. (A) Reduced 3.0-Pt/SiO_2–NO. (B) Oxidized 3.0-Pt/SiO_2–NO. (C) Reduced 0.6-Pt/SiO_2–NO. (D) Oxidized 0.6-Pt/SiO_2–NO. (E) 0.05-Pt/SiO_2–NO. (F) Oxidized 0.05-Pt/SiO_2–NO.

determined that the high-, medium-, and low-frequency components were due to crystallite facet faces, corners, and edges, respectively. The reducing pretreatment appears to result in platinum particles containing surface sites with a wider range of energies than does the oxidizing pretreatment.

There are also significant differences in the peak positions observed on the oxidized and reduced catalysts. In all five catalysts studied, the oxidizing pretreatment resulted in a higher frequency peak with a more consistent peak position than did the reducing pretreatment. This was especially true for the amine–nitrate samples ($2083 \pm 2\ cm^{-1}$). The reduced catalysts, however, show a much larger spread in peak position from 2057 to 2076 cm^{-1} depending on the loading. This effect is less apparent in the chloroplatinic acid samples, but it also should be noted that peaks for oxidized pretreatment are less symmetric than they are in the anime–nitrate samples, mainly due to the presence of a high-frequency shoulder at $\sim$2090 cm^{-1}.

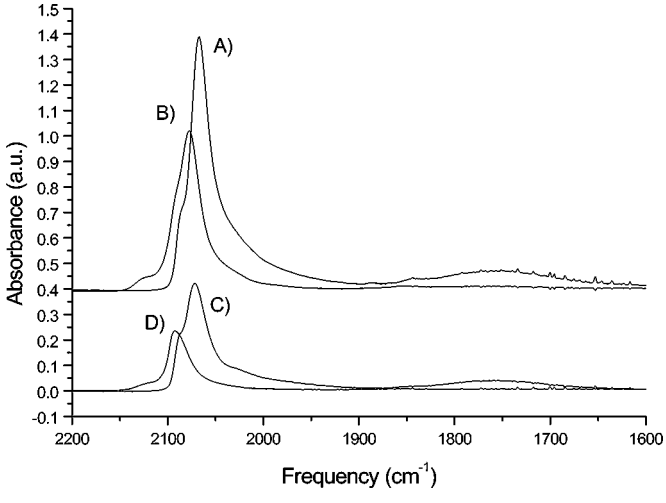

FIG. 2. Infrared spectra of CO adsorbed onto reduced and oxidized Pt/SiO_2 prepared form chloroplatinic acid. (A) Reduced 1.0-Pt/SiO_2–Cl. (B) Oxidized 1.0-Pt/SiO_2–Cl. (C) Reduced 3.14-Pt/SiO_2. (D) Oxidized 3.14-Pt/SiO_2–Cl.

The differences in infrared peak position for the reduced catalysts in this system can be explained by differences in the platinum particles sizes. Other authors (45) have observed a similar dependence of the CO stretching frequency on the dispersion of platinum particles. This phenomenon can be explained in terms of the classic Blyholder model (46) for the bonding of CO molecules to metal surfaces. In small platinum particles, the average number of platinum–platinum bonds per platinum atom is less than that in the larger particles. As a result, a higher metal electron density is available for back bonding into the $2\pi^*$ orbital of adsorbed CO molecules (46). The net result is a decrease in the C–O bond strength and a resulting decrease in the CO stretching frequency. Thus the smaller the particle size, the lower the stretching frequency for linearly bonded CO. This trend is consistent with the catalysts that underwent the reducing pretreatment. This explanation is also in agreement with previous studies that suggest that sites with lower platinum coordination (corners and edges) result in lower CO stretching frequencies (38, 47).

In addition to the typically observed linear and bridge-bonding peaks, both oxidized chloroplatinic acid samples contain a third peak at 2120 cm^{-1}. There has been some debate over the identity of this peak (48); however, the most common assignment is that of CO adsorbed on oxidized platinum (15, 20). The fact that this peak is observed only for catalysts after the oxidizing pretreatment is consistent with this peak assignment. However, the 2120-cm^{-1} peak was not observed in any of the catalysts prepared from the amine–nitrate salt. This observation suggests that the peak may instead be associated with some type of chlorinated or oxychlorinated platinum species. There is evidence from studies on carbonyl complexes that Pt(CO)–Cl_3 species show an absorption at 2121 cm^{-1} (49). In addition, the sample of catalyst 3.0-Pt/SiO_2–NO postimpregnated with chlorine showed a small shoulder at 2120 cm^{-1} after the oxidizing pretreatment. However, the absence of the 2120-cm^{-1} peak in all of the reduced samples suggests that the presence of chlorine assists in the formation of an oxidized form of platinum.

The relative consistency in peak position and the narrowness of the absorption peak observed on the oxidized catalysts can be explained by considering changes in the electronic state of platinum. Herz and Shinouskis (50) have proposed that the stretching frequency of CO linearly bonded to platinum can have a different value depending on the electronic state of the platinum site. In agreement with other authors they proposed that CO on fully reduced platinum results in a stretching frequency of 2070 cm^{-1} and that CO on oxidized platinum (Pt^{m+}, where $2 > m > 1$) results in a frequency of 2120 cm^{-1}. However, they also proposed two intermediate, partially oxidized, states of platinum ($Pt^{\delta+}$ and Pt^{n+}, where $1 > n > \delta$) which result in stretching frequencies of 2080 and 2095 cm^{-1}, respectively.

In this study, the CO stretching frequencies for all five catalysts were observed to be ~2080 cm^{-1} after the oxidizing pretreatment regardless of particle size. On the basis of the assignments by Herz and Shinouskis (50), this state is assigned to adsorption of CO on electron-deficient platinum, $Pt^{\delta+}$. This assignment can also be explained in terms of the Blyholder model. For all five catalysts, the oxidation resulted in platinum particles that were electron deficient. This lack of metal electrons decreased the amount of back bonding and resulted in a higher stretching frequency. The facts that all five catalysts showed the same frequency and that the FWHM decreased in each case imply that the effect of the electron deficiency overrides the particle size effect. All sites, including corners and edges, have become equivalent in energy, which is equal to that of $Pt^{\delta+}$.

This phenomenon also explains the observation that when a CO-saturated, oxidized sample was dosed with H_2 at room temperature, the spectrum observed for the reduced catalyst was reproduced. However, dosing the reduced catalyst with oxygen at room temperature had no effect. Hydrogen is able to remove the partial charge on the platinum particle that was imparted by the high-temperature oxidation, perhaps by removing residual surface oxygen. In addition, the high-frequency shoulders (~2090 cm^{-1}) observed on the chloroplatinic acid catalysts may be attributed to the Pt^{n+} state, where $1 > n > \delta$. In this case the chlorine impurities aide in the oxidation of the platinum sites to a greater extent than what was observed on the amine catalysts. However, because the high-frequency shoulders are also present after the reducing pretreatment, they may be the result of the electron-withdrawing power of chlorine itself.

In two of the three samples prepared from the amine salt, there is virtually no difference in the integrated CO peak areas observed after the reducing and oxidizing pretreatments. In the chloroplatinic acid samples and 0.05-Pt/SiO_2–NO catalyst, however, the integrated area of the peak after the oxidizing pretreatment was always less than that of the peak after the reducing pretreatment. In the chloroplatinic acid samples it is likely that the existence of oxidized platinum is affecting the overall adsorption of CO. The extinction coefficient for an oxidized site may be less than that for a reduced platinum site. In the low-loading nitrate sample, the difference in peak areas may be due to edge effects originating from the high dispersion of the platinum particles.

3.2. CO Desorption and the Coverage-Dependent Peak Shift

Thermal desorption of adsorbed CO was performed by recording IR spectra while heating the CO-saturated catalyst from room temperature to 400°C, as shown for the 1.0-Pt/SiO_2–Cl catalyst in Fig. 3. Figure 3 shows a large fluctuation in the baseline below 2000 cm^{-1} that becomes more intense as the temperature increases. This fluctuation is due

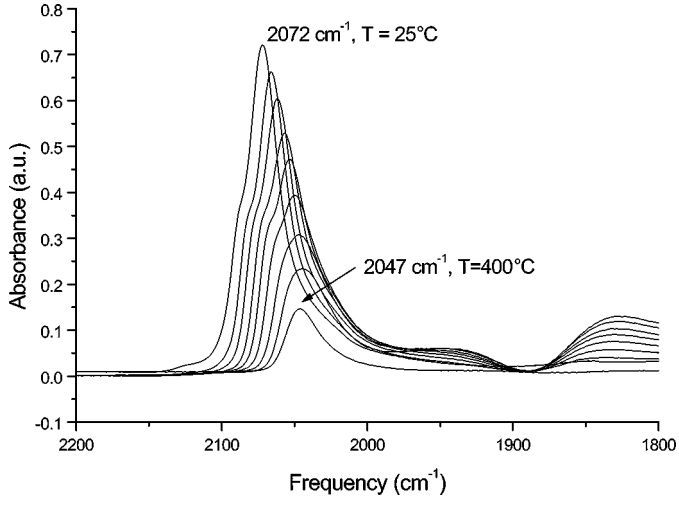

FIG. 3. Thermal desorption of CO from 1.0-Pt/SiO_2–Cl catalyst as measured by FTIR. Catalyst is heated from room temperature to 400°C.

to changes in overtone and combination bands from the silica support and not due to bridge-bonded CO species (12). During desorption, the linearly bonded CO peak position shifts 25 cm^{-1} to lower wavenumbers as the peak area decreases. This is in stark contrast to the constant stretching frequency observed during the adsorption of CO.

This coverage-dependent peak shift is well known and has been observed elsewhere on supported catalysts and single crystals (24, 27, 51–55). It has two primary components: the chemical shift and the dipole shift. The dipole shift occurs due to the interaction between adjacent vibrating dipoles on the catalyst surface. As the density of dipoles increases, the frequency of the vibration will also increase. This frequency shift due to dipole coupling only occurs if the frequencies of the interacting dipoles are nearly identical. The chemical shift, however, is due to changes in the electron distribution between CO and the metal as the surface density of adatoms increases and can be either positive or negative (56).

The inherent heterogeneity of the surface of a supported catalyst also may contribute to the observed peak shift. During thermal desorption, the CO molecules bonded to low-energy sites (which have a high stretching frequency) leave the surface first. This biased removal of high-frequency molecules may result in apparent peak shift as the molecules desorb (51). In this study, it was not possible to distinguish between the shift caused by surface heterogeneity and the shift due to coverage-dependent changes in the bonding properties of CO to the platinum surface. Both of these effects contribute to what is referred to here as the chemical shift. Thus the chemical shift measured in this research contains an additional contribution due to surface heterogeneity not typically observed on single crystals (12).

Surface heterogeneity may also complicate the measurement of the dipole shift due to the existence of intensity borrowing. It has been shown that lower frequency vibrators will transfer intensity to nearby higher frequency vibrators even if the separation in frequency is tens of wavenumbers (28, 57). The high-frequency band can effectively mask the low-frequency band. The net effect is that a portion of the chemical shift due to surface heterogeneity (as described in the previous paragraph) can be mistakenly attributed to dipole coupling (54, 57). Thus careful consideration must be given to the effects of surface heterogeneity on the coverage-dependent peak shift on supported catalysts.

An additional mechanism contributing to the infrared peak shift may also occur due to the change in temperature experienced by the sample in the desorption experiments. Jacob and Persson (58) have shown on Ru(001) that anharmonic coupling to a frustrated translational mode causes an 11-cm^{-1} red shift in the CO stretching frequency from 30 to 350 K. Data were not obtained for the temperature region above 350 K. However, assuming similar behavior on platinum and at a higher temperature range, a corresponding shift is not large enough to account for the observed peak shift in this system. More importantly, the full coverage frequency of CO at room temperature and at 250°C only varies by 1 cm^{-1} (see Table 2 and Fig. 13). Thus, it is unlikely that anharmonic coupling has a large effect on the CO frequency observed in this system.

3.3. *Dipole Coupling Simulations*

In order to gain a better understanding of the observed coverage-dependent peak shift, simulations were performed to investigate the effect of adsorbate geometry on the dipole shift contribution to the observed CO stretching frequency. The basic equations governing the behavior of interacting dipoles on a metal surface have been previously described (28–30). The stretching frequency of an ensemble of dipoles (ω) with a singleton frequency of ω_s, an electronic polarizability of α_e, and a vibrational polarizability of α_v (28) is given by

$$\left(\frac{\omega}{\omega_s}\right) = 1 + \frac{\alpha_v \Sigma_0}{1 + \alpha_e \Sigma_0}. \qquad [1]$$

The symbol Σ_0 is known as the dipole sum and is defined as

$$\Sigma_0 = \sum_{i \neq j} \frac{1}{r_{ij}^3} + \frac{1}{(r_{ij} + 2d)^3} - \frac{12d^2}{(r_{ij} + 2d)^5}. \qquad [2]$$

In this equation r_{ij} represents the distance between dipoles in the plane of the surface and d represents the distance between the center of the dipole and the image plane (29). This model assumes that all adsorbate molecules are oriented perpendicular to the metal surface.

In the original work of Persson and Ryberg, the value of the dipole sum was taken to be that of a complete monolayer (28). Mahan and Lucas (30) calculated the dipole sum for a partially filled monolayer by multiplying the dipole sum for the complete monolayer by the coverage. However, this assumes that the dipoles are arranged randomly on the surface. A further refinement of the dipole coupling model was made by Lauterbach *et al.* (56), who instead calculated the dipole sum directly over a 5000 × 5000 lattice of Ir atoms assuming the CO molecules were arranged in the $(\sqrt{3} \times \sqrt{3})R30^\circ$ overlayer structure. In this case, it was shown that the assumption of a random arrangement of adsorbed molecules predicted a higher frequency than was calculated for the $(\sqrt{3} \times \sqrt{3})R30^\circ$ structure at the same coverage.

Simulations in this study were performed by defining a lattice that represents a platinum (111) surface. CO molecules were placed on the lattice in specified geometries. The resulting CO stretching frequency was calculated based upon the position of all molecules on the lattice. The simulations were typically performed on lattices ranging from 10 × 10 to 50 × 50 cells without periodic boundaries.

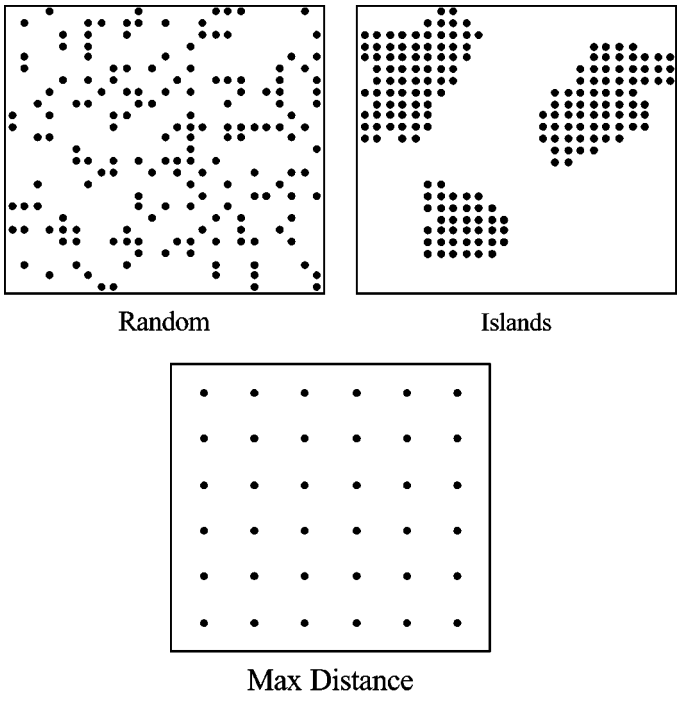

FIG. 4. Examples of the three adsorbate geometries used in the dipole coupling simulations.

Based on the size of the platinum atom, this corresponds to facet dimension of 3–14 nm, which is a reasonable size for supported platinum particles (43). The distance to the image plane was chosen to be $d = 1.0$ Å, and the electronic polarizability was chosen to be $\alpha_e = 2.54$ Å^3 (29, 56). The vibrational polarizability was used as a fitting parameter (56).

The three basic adsorbate geometries used in the simulations are shown in Fig. 4. In the "island" geometry, CO molecules were allowed to cluster together into close-packed islands. The "maximum distance" geometry represented the opposite situation, in which CO molecules repel each other and maximize the distance between themselves. The "random" geometry placed CO molecules on the lattice randomly. The stretching frequency of the ensemble was then calculated as a function of coverage in small steps up to a fully covered surface. CO molecules were only allowed to adsorb onto on top positions, and coverage is defined as the number of CO molecules on the surface divided by the total number of adsorption sites (platinum atoms).

Figure 5 shows the results of these simulations on a 50×50 Pt(111) lattice. As predicted by Mahan and Lucas, random adsorption results in approximately linear dependence upon coverage (30). A slight decrease in slope at high coverage is most likely the result of edge effects due to the use of nonperiodic boundaries. The island geometry resulted in a sharp rise in peak position up to about 10% coverage and then a slow rise in peak position as the surface saturates further. The maximum distance geometry showed a slower rise in peak position at lower coverage up to a coverage of 50%, in which case the maximum distance and random profiles converged. For all three cases the value of the vibrational polarizability was chosen to be 0.21 Å^3 and the singleton frequency was chosen to be 2040 cm^{-1}. These values gave the best agreement with the peak positions observed during the thermal desorption experiment and are in agreement with values used by other authors ($\alpha_v = 0.057$–0.34 Å^3, and $\omega_s = 2034$–2065 cm^{-1}) (53, 56). It should be noted that the overall shape of the plots shown in Fig. 5 is a very weak function of the polarizabilities, the singleton frequency, and the platinum surface geometry ({100} or {111}). These parameters only significantly affect the range of peak positions.

These simulations were performed assuming the surface is energetically homogeneous. The presence of defect sites with different energies would not significantly alter the results of the simulation. As mentioned in Section 3.2, a peak shift is not observed between dipoles with different stretching frequencies. Thus a molecule adsorbed on a defect site would contribute to an increase in coverage, but not an increase in frequency. Thus the presence of defects would dilute the effects predicted by these simulations. For example, the island profile would approach the random profile. The same effect can be achieved if more nucleation sites are chosen in the island geometry simulation (i.e., more islands with smaller average dimensions.) The simulations performed in this study show the maximum shift that can be observed for a given coverage and geometry. The basic trends observed remain unaffected by surface heterogeneity.

Also plotted in Fig. 5 are the peak positions obtained from the thermal desorption experiment shown Fig. 3. As

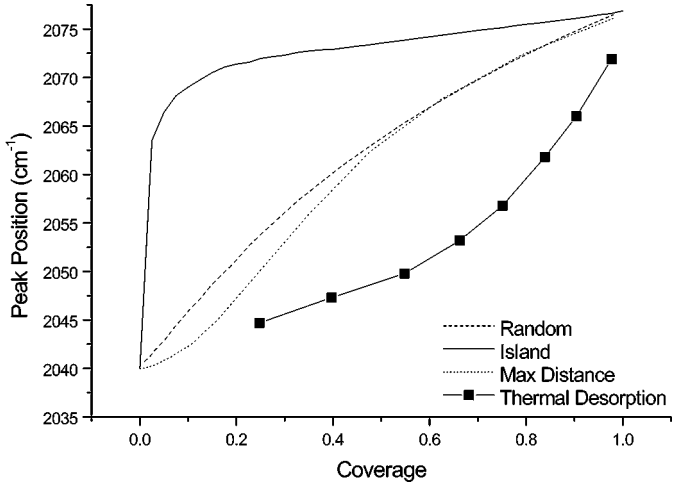

FIG. 5. Results of the dipole coupling simulations for the three adsorbate geometries shown in Fig. 4 with $\alpha_e = 2.54$ Å^3, $\alpha_v = 0.21$ Å^3, and $\omega_s = 2040$ cm^{-1}. Also included are the peak positions measured during the thermal desorption shown in Fig. 3.

is evident from the figure, the peak positions observed from thermal desorption all fall below the positions predicted by any of the three adsorption geometries. Because the max distance geometry is by definition a state in which the CO molecules are as far away from each other as possible, it is impossible to access the area of the graph beneath this line if dipole–dipole coupling is the only mechanism contributing to the coverage dependent peak shift. As mentioned earlier, the other main component of the coverage-dependent peak shift is known to be the chemical shift. In order to fully understand the change in peak position during thermal desorption, the coverage dependence of the chemical shift in this system must be quantified.

3.4. Isotope-Mixing Experiments

Isotope-mixing experiments can be used to separate the dipole shift from the chemical shift and other contributions to the stretching frequency of molecules adsorbed on metal surfaces. The difference in the reduced mass of two isotopes such as $C^{16}O$ and $C^{18}O$ results in the two molecules having different stretching frequencies. This frequency difference prevents the dipoles of isotopically different species from coupling. Thus, the relative amount of the two isotopes on the surface determines the extent of dipole coupling. The chemical shift, however, is a function of the bonding properties of the metal substrate and is therefore independent of isotopic substitution in the adsorbate layer (59). If a series of isotopic mixtures is dosed onto a metal surface at a given total coverage, the infrared stretching frequency can be measured as a function of the isotopic composition. The data can then be extrapolated to the case of an infinite dilution of $C^{16}O$ in $C^{18}O$. The resulting frequency is that of a molecule of $C^{16}O$ in the absence of dipole coupling. If the entire experiment is repeated for the case of different total coverages of CO, the chemical shift can also be determined as a function of coverage (27, 54, 56).

Isotope-mixing experiments have been performed extensively on single-crystal surfaces (27, 54, 56). Experiments on supported catalysts, however, are rare and typically only measure the dipole shift at full coverage (60–62). To our knowledge, this work gives the first example of the chemical shift calculated for a supported catalyst. Due to the rapid rate of adsorption compared to diffusion (37, 38, 42), low-pressure dosing of the isotopic mixture does not result in local coverages less than unity and the chemical shift cannot be measured. In order to achieve a lower surface coverage, a mixture of $C^{16}O$ and $C^{18}O$ was passed over the catalyst at a pressure of 10 mTorr. The temperature of the system was varied in the region above the CO desorption temperature to allow for different total surface coverage. Podkolzin *et al.* (37) have shown that equilibration in this manner at high temperature on supported catalysts results in adsorption and desorption behavior similar to that observed on single crystals.

In this experiment, each of the five catalysts was equilibrated with a mixture of $C^{16}O$ and $C^{18}O$ over a temperature range of 200–500°C. At each coverage, the total flow rate, system pressure (10 mTorr), and temperature were kept constant and the percentage of $C^{18}O$ in the stream was varied from 0 to 100% in steps of 20%. FTIR spectra were collected at each isotope mixture. The temperature was then changed to achieve a different surface coverage, and the catalyst was again exposed to a series of isotope mixtures. For example, on the 3.0-Pt/SiO_2–NO sample, equilibration at 318°C resulted in a coverage of 0.87 and equilibration at 360°C resulted in a coverage of 0.64. The total coverage achieved at each temperature was estimated by comparing the total integrated area of the 100% $C^{16}O$ peak to the area found at 200°C where the coverage is unity. For these experiments, we have assumed that integrated infrared peak area is proportional to coverage (29, 63). Figure 6 contains an example of the infrared spectra obtained from the 0.6-Pt/SiO_2–NO catalyst at 200°C (corresponding to full coverage). Each sample was observed to equilibrate very quickly between measurements, and it was found that waiting 30 s between mixtures yielded reproducible results. We reiterate that for the reasons discussed in Section 3.2, we expect the temperature dependence on the stretching frequency to be on the order of only a few wavenumbers and thus the observed frequency shift is due entirely to coverage-dependent effects.

The dipole and chemical shifts for each catalyst were determined by plotting the position of the $C^{16}O$ peak as a function of the percentage of $C^{16}O$ in the mixture.

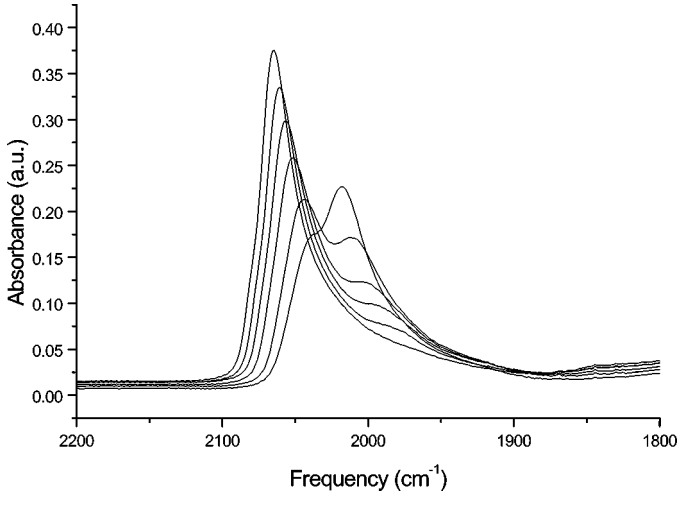

FIG. 6. Example of data from the isotope-mixing experiments. These spectra were collected on the 0.6-Pt/SiO_2–NO sample at 200°C, which corresponds to full coverage. The spectra shown correspond to 100% $C^{16}O$, 80% $C^{16}O$ with 20% $C^{18}O$, 60% $C^{16}O$ with 40% $C^{18}O$, 40% $C^{16}O$ with 60% $C^{18}O$, 20% $C^{16}O$ with 80% $C^{18}O$, and 100% $C^{18}O$ from left to right. Extrapolation to zero coverage of $C^{16}O$ results in a dipole singleton frequency of 2041 cm^{-1}. Based on the 100% $C^{16}O$ frequency of 2067 cm^{-1}, the resulting dipole shift for this sample is 26 cm^{-1}.

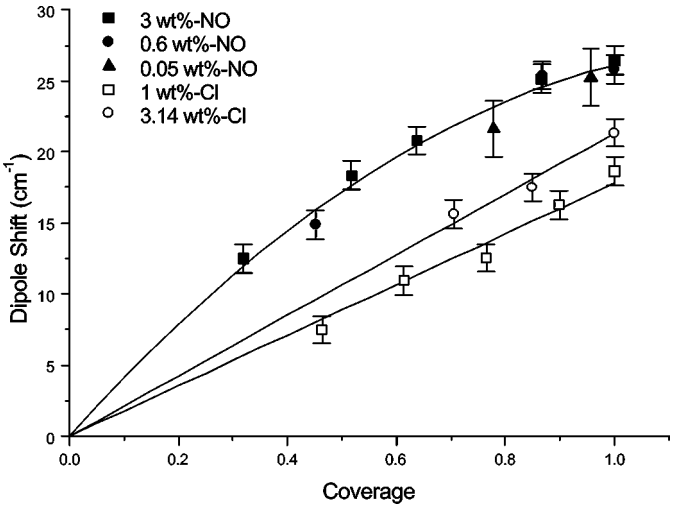

FIG. 7. Comparison of the dipole shift as measured in the isotope-mixing experiment for the five different catalysts examined in this study. Coverage was varied by heating the sample above the onset of desorption for CO. Each point is obtained via the method described in the text and in the caption of Fig. 6.

Extrapolating each line to 0% $C^{16}O$ results in the peak position of $C^{16}O$ on the catalyst surface in the absence of dipole coupling. This frequency is referred to in this work as the dipole singleton frequency. The dipole shift can then be determined by subtracting the dipole singleton frequency from the frequency observed with 100% $C^{16}O$ at the same coverage. For all five catalysts, plots of the peak position versus isotope mixture were highly linear. The R^2 value for most plots exceeded 0.99 and in all cases exceeded 0.96.

Figures 7 and 8 summarize the results of the isotope-mixing experiments. As can be seen from Fig. 7, the dipole shift for all catalysts is proportional to coverage. Data for all three amine–nitrate precursor catalysts follow the same trend and show maximum shift of 26 cm^{-1}. The chloroplatinic acid samples also show linear behavior in coverage, but the maximum shift is less than what is observed in the amine–nitrate samples at 21 and 18 cm^{-1} for the 3.1 and 1.0 wt% catalysts, respectively. The presence of chlorine impurities may be the cause of the smaller dipole shift. In this case the effect of chlorine would be to occupy adsorption sites, which would disrupt the CO adlayer and increase the average distance between CO molecules. However, this difference in total dipole shift may also indicate a difference in particle morphology (62). For example, the amine–nitrate catalyst particles may contain a larger percentage of Pt(111)-type facets that would allow closer packing of the CO molecules and therefore greater dipole–dipole interaction.

A comparison of the dipole shift measured for the anime–nitrate catalysts (solid symbols in Fig. 7) and peak positions predicted by the random geometry dipole coupling simulation (dashed line in Fig. 5) reveals that the two data sets follow the same trend. Quantitative agreement between the two profiles is difficult due to the uncertainty of accurately measuring the singleton frequency on supported catalysts and the potential for surface heterogeneity. However, under the conditions of the simulation shown in Fig. 5 ($\alpha_e = 2.54$ Å^3, $\alpha_v = 0.21$ Å^3, and $\omega_s = 2040$ cm^{-1}), there is quantitative agreement between the Random geometry simulation and the results of the isotope-mixing experiment for the anime–nitrate catalysts as shown in Fig. 7.

Figure 8 shows the dependence of the dipole singleton frequency on coverage for each of the five catalysts in this study. The dipole singleton frequency is defined here as the frequency of $C^{16}O$ observed when the effect of dipole coupling has been completely canceled out by infinite dilution in $C^{18}O$. The dipole singleton frequency is then equal to the sum of the chemical shift and the stretching frequency of $C^{16}O$ in the extrapolation to zero coverage (commonly referred to as the singleton frequency). Thus, in effect, Fig. 8 shows the dependence of the chemical shift on coverage for each sample since the singleton frequency is by definition a constant for each sample. These data are reported in this manner due to the difficulty in accurately measuring the singleton frequency on supported catalysts, as mentioned previously. Each catalyst shows a sharp increase in the chemical shift at high coverages (above 80%). However, each plot shows very little change in the shift from 30 to 80% coverage. Data from both the chloroplatinic acid catalysts and the most highly loaded amine–nitrate catalyst all follow the same trend. The remaining two amine–nitrate samples show lower peak positions and a slightly lower overall shift.

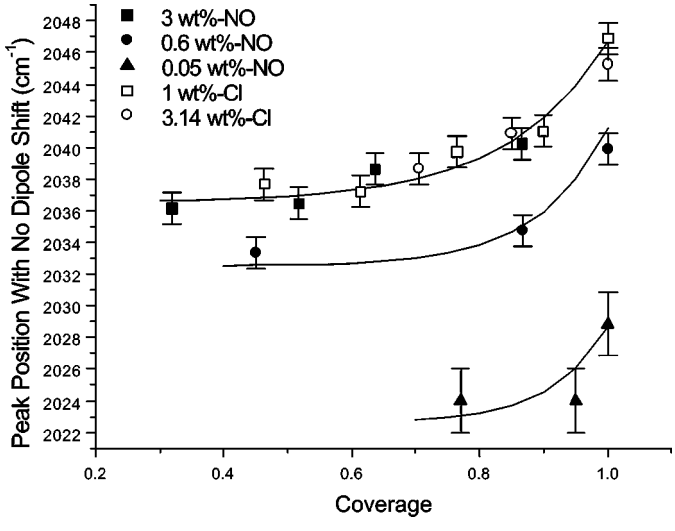

FIG. 8. Comparison of the chemical shift measured in the isotope-mixing experiment for the five catalysts in this study. Due to the uncertainty of the singleton frequency for each sample, the CO stretching frequency is shown with the effect of dipole coupling removed by isotopic substitution. Coverage was varied by heating the sample above the desorption temperature for CO. Each point is obtained via the method described in the text and in the caption of Fig. 6.

The shape and range of all three curves are essentially the same, but the two low loading amine–nitrate samples appear to be approaching a different singleton frequency. This is consistent with the results of the CO adsorption experiments on the reduced catalysts that showed a correlation between peak position and particle size. In general, there is no significant difference in the chemical shift behavior of the five catalysts. In all cases, the measured chemical shift was 8–10 cm^{-1} and showed the most change at high coverage. The dipole shift, however, shows both a larger range (15–25 cm^{-1}) and a stronger dependence on the total coverage. Both the dipole shift and the chemical measured in these experiments are comparable to those observed on Pt(111) single crystals (54).

A second method of obtaining the chemical shift is also possible. If we assume that thermal desorption is randomly removing CO molecules from the platinum surface, then in the absence of the chemical shift, the peak position profile observed during thermal desorption should match the profile simulated from the random geometry (Fig. 5). Based on this assumption, the difference in frequencies between the thermal desorption and random geometry profiles seen in Fig. 5 is entirely the result of the chemical shift. Thus, if the two profiles are subtracted from one another, the resulting profile contains only the chemical shift as a function of coverage. Figure 9 shows the result of such a calculation for a sample of 1.0-Pt/SiO_2–Cl. For this calculation the fitting parameters used for the dipole coupling simulation were adjusted slightly from the values used in Fig. 5 due to a change in the sample used in the experiment. This sample had a history and a slightly different thermal desorption profile than the samples shown in Figs. 4 and 5. However, the resulting parameters were well within their expected ranges. For the sake of comparison, Fig. 9 also repeats the dipole singleton frequencies obtained from the isotope-mixing experiment (from Fig. 8). The agreement between the thermal desorption data and the isotope-mixing data when the effect of dipole coupling has been removed (Fig. 9) verifies the claim made in Section 3.3 that the discrepancy between the peak positions observed during thermal desorption and predicted by the dipole coupling simulation is entirely due to the chemical shift. It is also interesting to note that the curve produced from the thermal desorption data suggests a minimum may exist in the chemical shift as a function of coverage. This type of behavior was also observed on a Pt(111) single crystal by Tüshaus *et al.* (54), although the minimum in the chemical shift observed in their data occurred at a slightly lower coverage (0.35 as opposed to 0.5). This method, although less rigorous than isotopic mixing, provides a straightforward, simple way in which to estimate the chemical shift as a function of coverage on supported catalysts.

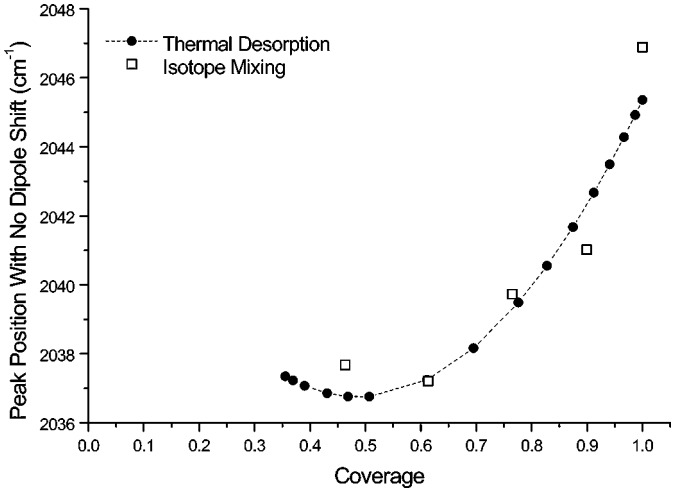

FIG. 9. Comparison of the chemical shift obtained through the isotope-mixing experiment and the chemical shift obtained by subtracting the simulated dipole shift ($\alpha_e = 2.54$ Å^3, $\alpha_v = 0.125$ Å^3, and $\omega_s = 2045$ cm^{-1}) from the measured peak position observed during thermal desorption of CO from 1.0-Pt/SiO_2–Cl.

As mentioned in Section 3.2, surface heterogeneity must be considered in the interpretation of the dipole and chemical shifts. Specifically, heterogeneity may cause a portion of the chemical shift to be attributed to the dipole shift through intensity borrowing. This was done by Crossley and King on a recrystallized Pt(111) ribbon (27), but later corrected by Tüshaus *et al.* using a more well-defined Pt(111) single crystal (54, 57). In this study, however, intensity borrowing does not appear to have affected the results. First, the measured values of the chemical and dipole shift in this study agree within a few wavenumbers to those measured by Tüshaus *et al.* (54). In contrast, Crossley and King measured a dipole shift of 35 cm^{-1} with no chemical shift (27). Second, as previously mentioned, the profile for the dipole shift as a function of coverage agrees very well with the random geometry dipole simulation, which was performed assuming a well-defined surface. Finally, in the isotope-mixing experiments of Crossley and King, a significant amount of broadening occurred at intermediate mixtures of the two CO isotopes. The peak width almost doubled and a clear shoulder was present (27). In hindsight, it is clear that a second, lower frequency band was present in the spectrum (57). The isotope-mixing experiments in this study show a line broadening of only a few wavenumbers as the concentration of $C^{18}O$ increases (see Fig. 6). The combination of these three observations strongly implies that the dipole shift measured in this study does not contain a significant contribution from the chemical shift due to heterogeneity.

The fact that intensity borrowing does not seem to operate in this system has interesting implications. One explanation is that all sites on a single platinum particle have approximately the same energy and thus all sites can couple and contribute to the frequency shift. This explanation is consistent with the work of Welch *et al.* (62) on the

EUROPt3 catalyst where it was concluded that the supported catalyst contained only one type of adsorption site. If there are multiple types of adsorption sites, and if the energy difference between the sites is small, then the dipole coupling may be strong enough for the dipole-induced frequency shift to occur. This explanation is consistent with experiments on Pt(533) which gave evidence for strong dipolar coupling between step and terrace sites (64). If this explanation is valid, then the width of the adsorption band observed in the CO adsorption study (see Section 3.1 and Figs. 1 and 2) is due mainly to the particle size distribution, i.e., interparticle heterogeneity, not intraparticle heterogeneity.

3.5. Oscillatory Reaction Behavior

In addition to adsorption and desorption experiments, the oxidation of carbon monoxide was studied in the oscillatory regime. The oscillatory behavior and parameter space for the 3.1-Pt/SiO_2–Cl catalyst have been previously reported at a total pressure of 1–10 Torr (9). The reaction over this catalyst was observed to oscillate over a wider range of temperature and CO/O_2 ratio than a Pt(100) single crystal. In particular, the single crystal was only observed to oscillate at CO/O_2 ratios below 0.1. The supported catalyst, however, showed oscillatory behavior up to a CO/O_2 ratio of 1.7. Oscillations were, in general, observed for temperatures between 190 and 270°C with a period of 120 to 35 s, respectively. Infrared spectra of the catalyst under reaction conditions showed that the CO coverage on the catalyst that varied between 3 and 5% during the oscillation. In addition, the IR peak position of the adsorbed CO was within a few wavenumbers of the value observed when the surface was saturated with CO (9).

In this study, before the reaction each catalyst was reduced in 10 mTorr of H_2 for 30 min at 200°C and then oxidized at the same pressure for 30 min at 300°C. The catalyst was then cooled in vacuum to the reaction temperature. Reactions were run at a pressure of 1.2–1.5 Torr at a specified O_2/CO ratio. The temperature was slowly raised and the onset and eventual extinction of oscillations were observed by monitoring the production of CO_2 with the mass spectrometer. Simultaneously, infrared spectra were collected from the sample during the reaction. In all cases the oscillations observed were isothermal. The temperature, as measured by the thermocouple in contact with the catalyst wafer, varied by no more than 1 K during the period of the oscillation.

Figures 10–13 show examples of the oscillations observed in this study as monitored by both mass spectrometry and FTIR. In Figs. 10 and 12, the coverage of CO as a function of time is estimated by dividing the integrated peak area for the linearly bound CO observed during the reaction by the area found when the catalyst is saturated with CO. Figures 10 and 12 clearly show the inverse relationship

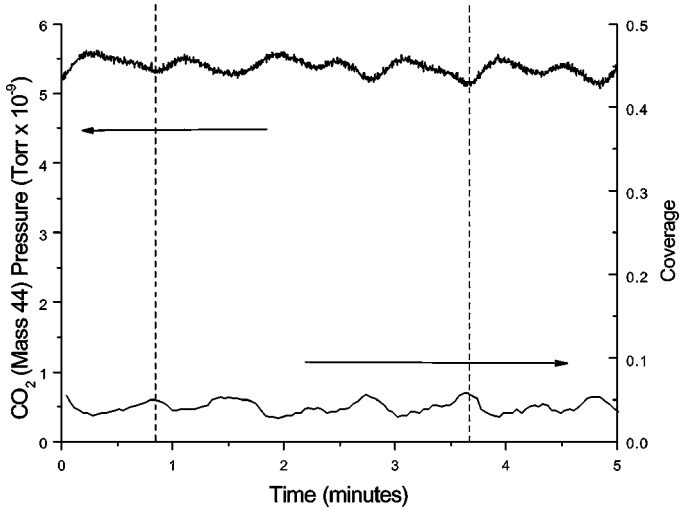

FIG. 10. Kinetic oscillations in oxidation of carbon monoxide as observed by both MS and FTIR. The oscillations were obtained over the 0.6-Pt/SiO_2–NO catalyst at $P = 1.3$ Torr, $T = 245$°C, and $O_2/CO = 3.0$. The coverage is obtained by the ratio of integrated IR peak areas.

between the amount of CO on the catalyst and the production of CO_2. In addition, the coverage of CO is seen to oscillate between 1 and 30% during the reaction. Although not shown, the gas-phase CO concentration in the reactor also oscillated as a function of time. The gas-phase CO oscillations were in phase with the oscillations of CO on the surface and 180° out of phase with the concentration of CO_2. Oscillations in the gas-phase concentration of O_2 were either not observed at all or small in amplitude and in phase with the oscillations of CO. This was expected considering the reaction was typically run in excess of oxygen. Figure 12 also shows the effect of switching off the flow of oxygen during the reaction at the 5-min mark. The coverage

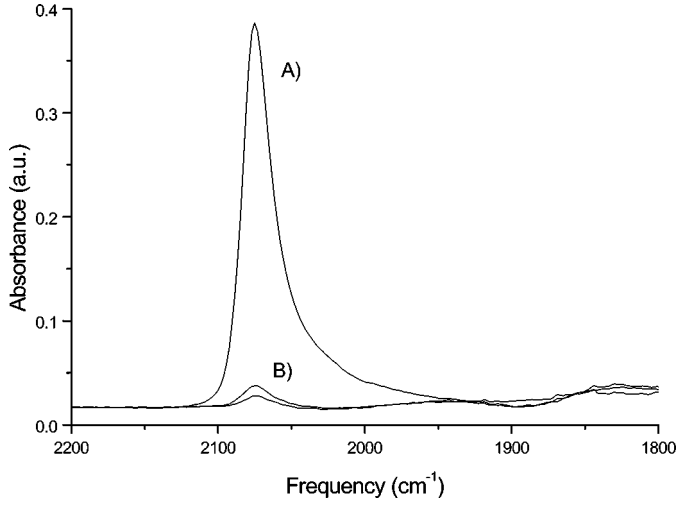

FIG. 11. Infrared peak obtained during the kinetic oscillations shown in Fig. 10. Peak A represents full coverage by CO. Peaks B were observed under oscillatory conditions.

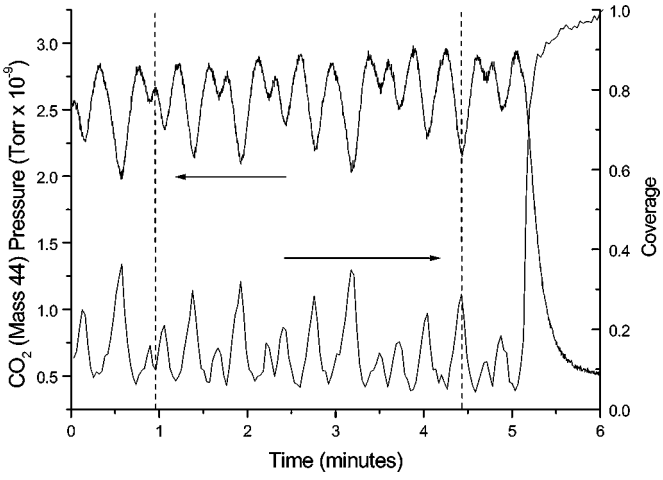

FIG. 12. Kinetic oscillations observed over 3.14-Pt/SiO_2–Cl. The reaction conditions were $P = 1.3$ Torr, $T = 245°C$, $O_2/CO = 3.0$. At the 5-min mark, oxygen flow to the reactor ceased.

of CO reaches saturation and the production of CO_2 drops to zero in just a few seconds.

Of the five catalysts studied, four were observed to display oscillatory behavior. The catalyst that failed to oscillate was the 0.05-Pt/SiO_2–NO catalyst. The reaction rate measured on the 0.05-Pt/SiO_2–NO was very low compared to the other four catalysts. Any oscillations that may have occurred on this catalyst were most likely too small in amplitude to detect. The remaining four catalysts all showed behavior very similar to that of the 3.1-Pt/SiO_2–Cl catalyst studied previously (9). There were no significant differences in the parameter space, oscillation shape, or period between the four catalysts studied.

Figures 11 and 13 show examples of IR spectra obtained during the oscillations for both the amine–nitrate and chloroplatinic acid samples. The most notable feature is the lack of a large peak shift in the stretching frequency during the oscillation, even though the coverage is low (1 to 30%). The chloroplatinic acid samples showed an $\sim$5 cm^{-1} peak shift during the oscillations, while the amine–nitrate catalysts showed only a 1- to 2-cm^{-1} shift. This is in stark contrast to the 25-cm^{-1} coverage-dependent peak shift observed in the CO adsorption and desorption studies. If CO existed in a random configuration on the catalyst surface during reaction, frequency is predicted to be 2055 cm^{-1} at 30% coverage (see Fig. 5), not 2071 cm^{-1} as seen in Fig. 13.

3.6. Evaluation of Previously Proposed Feedback Mechanisms

On the basis of our results, the two most commonly cited mechanisms used to explain the kinetic rate oscillations in the oxidation of carbon monoxide on supported platinum catalysts, the carbon model and the reduction/oxidation model, can be ruled out as the driving forces for the oscillations observed in this system. First, simulations performed using both models predict the surface coverage of CO to cycle between 0 and 100% during the oscillation (8, 15). Clearly, under our reaction conditions, the coverage instead cycles between 1–5 and 5–30% depending on the catalyst and its pretreatment. In addition, the period of oscillations is on the order of 35 to 120 s as opposed to the several minutes predicted by either of these two models.

Some groups have observed oscillations in the peak occurring at 2120 cm^{-1} attributed to CO on oxidized platinum and have suggested that this is proof of the oxidation/reduction model (15, 20). In this study, however, the 2120-cm^{-1} peak was only observed in the chloroplatinic acid catalysts, while oscillations were observed in all moderately loaded catalysts, regardless of the precursor. Even in the chloroplatinic acid samples, the 2120-cm^{-1} peak was not observed to oscillate (see Fig. 13). Clearly, this peak belongs to a spectator species and is not necessary for the oscillations observed on this catalyst at moderate pressure.

The carbon model can be ruled out based on coking experiments performed on Pt catalysts by Anderson *et al.* (65). They found that as coke was deposited on the platinum surface, the CO stretching frequency decreased by $\sim$20 cm^{-1}. This shift was attributed to a decrease in the dipole coupling between CO molecules. In the current study, the CO stretching frequency was only observed to decrease by 5 cm^{-1} or less. Thus, it seems unlikely that either the carbon or the oxidation/reduction mechanism is responsible for the oscillations observed over this catalyst.

3.7. CO Island Formation Model

The relatively small infrared peak shift observed during the oscillations suggests that the CO present on the surface

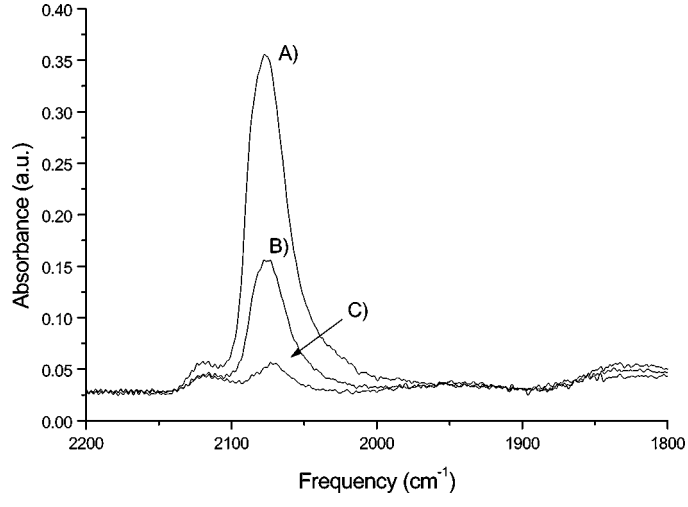

FIG. 13. Infrared spectra of adsorbed CO taken during the oscillations shown in Fig. 12. Spectrum A represents full coverage and was taken at the 6-min mark in Fig. 12. Spectrum B was collected during the low-reactivity portion of the oscillation. Spectrum C was collected during the crest of the oscillation.

during the reaction must exist in the form of close-packed islands. The isotope-mixing experiments (Section 3.4) show that dipole coupling is the primary contributor to the observed coverage-dependent peak shift for the catalysts in this study. This implies that during oscillations, the adsorbed CO molecules experience a significant amount of dipole coupling. The islands maintain a local high coverage of CO that results in strong dipole coupling, even though the total coverage is low. Several others have observed the same phenomenon under both steady-state and oscillatory conditions and have come to the same basic conclusion (1, 23, 24).

Additional evidence of the existence of islands during the oscillations was obtained by replacing a portion of the inlet CO with isotopically labeled $C^{18}O$ under reaction conditions. The addition of the isotope causes the $C^{16}O$ peak to shift down in frequency by 17 cm^{-1} as shown in Fig. 14. This shift also implies that the $C^{16}O$ molecules are highly dipole coupled (and thus close packed) during the oscillations, even in the presence of oxygen. It was shown in Section 3.1 that an oxidizing pretreatment results in an increase in the stretching of adsorbed CO. Under reaction conditions, there may be a slight effect of oxygen on the frequency of CO (which would account for the observation in Fig. 14 that peak B is blue shifted 2 cm^{-1} from peak A). However, the 17-cm^{-1} shift upon the addition of $C^{18}O$ to the reaction mixture conclusively proves that islands of CO must exist on the catalyst surface during the oscillations.

Further evidence to support the existence CO islands can be found by comparing the peak position observed during the oscillations to the peak positions predicted by

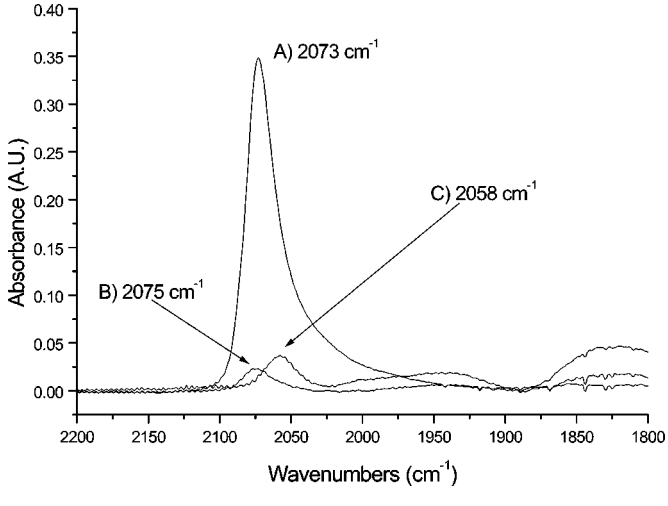

FIG. 14. Result of adding $C^{18}O$ to the reaction mixture under oscillatory conditions on 0.6-Pt/SiO_2–NO at 245°C and 1.2 Torr. (A) Full coverage of $C^{16}O$ with no O_2 flow. (B) Oscillatory condition, 3 : 1 ratio of $O_2 : C^{16}O$. (C) Oscillatory condition with isotope added, 3 : 0.5 : 0.5 ratio of $O_2 : C^{16}O : C^{18}O$. The 17-cm^{-1} shift upon the introduction of $C^{18}O$ indicates that CO is present in the form of densely packed islands under oscillatory conditions.

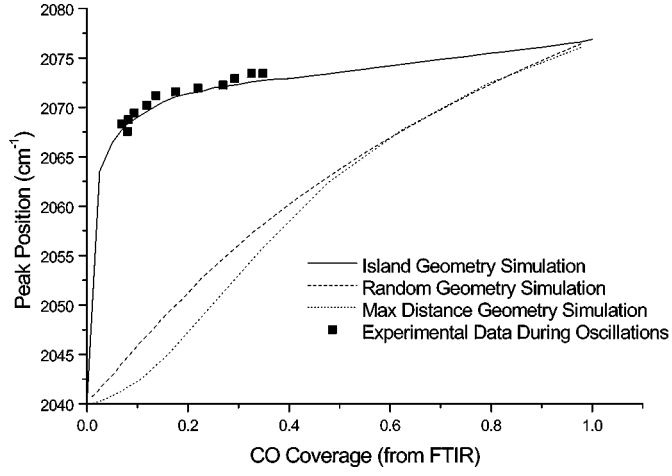

FIG. 15. Comparison of dipole coupling simulation results for the island geometry and the peak positions obtained during oscillations over 1.0-Pt/SiO_2–Cl.

the dipole coupling simulations. Figure 15 shows the results of the dipole coupling simulations for the three previously specified adlayer geometries. Figure 15 also shows the peak positions measured during oscillations on the 1.0-Pt/SiO_2–Cl catalyst. Clearly, there is excellent agreement between the experimental data and the predictions based upon the island geometry.

It is widely accepted that the oxidation of CO over platinum typically takes place in one of two reactive states. In one state, the platinum surface is completely covered with CO and the reaction rate is low due to the inhibition of O_2 adsorption. In the second state, the surface is completely covered with O atoms and the reaction rate is high (14, 24, 25). In this study, it has been shown that the surface CO exists in densely packed CO islands during the reaction. During the oscillations, these islands change in size and thus poison a different percentage of the active sites. In this way, different parts of the same platinum particle exist in the oxygen-rich and the CO-poisoned state simultaneously, which results in an overall coverage of 1–30 %. Some CO_2 production also may be occurring at the periphery of the CO islands. However, because the coverage of CO and the production of CO_2 are related in an inverse manner (see Figs. 10 and 12), the majority of the CO_2 production must occur in the O-rich portion of the particles. Gas-phase CO adsorbs onto the O-rich phase and rapidly reacts to form CO_2. In this mechanism, the CO islands act as an inactive region on each particle that changes the total reactive area by oscillating in size over time.

On very small (<2-nm) particles, the formation of islands becomes difficult due to the small number of total atoms. However, it should be noted that the catalyst with smallest particle size (0.05-Pt/SiO_2–NO) did not display oscillatory behavior. In addition, TEM showed that the other two amine–nitrate catalysts both had a broad distribution

of particle diameters. Thus, the island formation that leads to reaction rate oscillations may be occurring exclusively on the larger platinum particles.

3.8. The Possibility of Mass Transfer Limitations

An additional issue that has not been discussed up to this point is the possibility that the oscillations observed in this system are the result of mass transfer limitations. It is possible that the behavior of the surface CO observed by FTIR is due to a layer of the catalyst pellet in which all the platinum particles are fully covered with CO. There is still some debate in the literature over whether both external and internal diffusion are negligible in this reaction. One study found that external transfer limitations can limit the reaction rate over platinum foils and supported catalysts at pressure as low as 500 mTorr (66). Other studies have claimed the reaction is free from both internal and external mass transfer limitations at pressures between 1 and 10 Torr (15) and at atmospheric pressure (24).

Turnover frequencies were not measured in this study due to an unknown amount of gas phase bypassing of the catalyst pellet. However, based on our observation of this catalyst system, we believe that the oscillations observed are kinetic in nature. We rule out mass transfer limitations for the following reasons: (i) As can be seen from Fig. 12, when O_2 is turned off, the catalyst saturates with CO very quickly. At 1 Torr, CO is able to diffuse into catalyst in just a few seconds. The oscillations, however, are on the time scale of 30 to 120 s, much slower than the time scale on which diffusion acts in this system. (ii) The oscillations in the gas-phase concentrations of CO and CO_2 as well as in the surface coverage of CO are completely synchronized. If the system were diffusion limited, there would be a time lag as gases diffused into and out of the pellet. (iii) If diffusion were controlling the oscillations, there would always be platinum particles at full coverage inside the pellet and the CO stretching frequency would not change during the oscillations. We do observe a reproducible 1- to 5-cm^{-1} shift in the peak position during the oscillations. (iv) An experiment was performed in which the 1.0-Pt/SiO_2–Cl catalyst was diluted 10 to 1 in unimpregnated support and pressed into an IR pellet. IR spectra produced under reaction conditions were identical in shape, coverage, and frequency to those produced by the undiluted catalyst. (v) The stoichiometry of the reaction requires that two CO molecules be consumed for every O_2 molecule that participates in the reaction. If concentration gradients exist inside the pellet, the ratio of O_2 to CO would necessarily increase toward the center of the pellet. If a region of the pellet were completely CO poisoned, it would have to be the outside of the pellet. The thickness of this layer, and thus the observed partial coverage of CO, would then be a strong function of the O_2/CO ratio in the gas phase. In contrast, our experiments show no such correlation.

3.9. The Effect of the Catalyst Precursor

It was observed that the type of precursor used in catalyst synthesis (chloroplatinic acid or tetraammine platinum(II) nitrate) affected the amplitude of the oscillations observed in this study. The small-amplitude oscillations typified by Figs. 10 and 12 are typical of those observed on the amine–nitrate catalysts. The two chloroplatinic acid catalysts, however, showed oscillations typified by Figs. 12 and 13. The oscillations have much larger amplitudes and the change in the coverage of surface CO is correspondingly much larger (5–30%).

Although the amplitude of the oscillations that occur on the amine–nitrate and chloroplatinic acid catalysts is initially different, similar behavior was obtained when the pretreatment of the chloroplatinic acid samples was adjusted. When the catalysts were oxidized at 450°C and then cooled to the reaction temperature, the smaller amplitude oscillations with a correspondingly low surface coverage were produced. Figure 16 compares oscillations observed over the same catalyst sample with different pretreatments. The high-temperature (450°C) oxidation resulted in a 50% reduction in the oscillation amplitude. In addition, the IR spectra taken during the oscillations were virtually identical to those observed over the amine–nitrate catalysts. It should be noted, however, that the changes induced in the catalyst by the high-temperature oxidation were not reversible. Once the catalyst reached the low-amplitude state, the high-amplitude state could not be reproduced by treatment with hydrogen. It should also be noted that the total integrated peak area of CO on a saturated surface did not change as a result of the different pretreatments. Thus

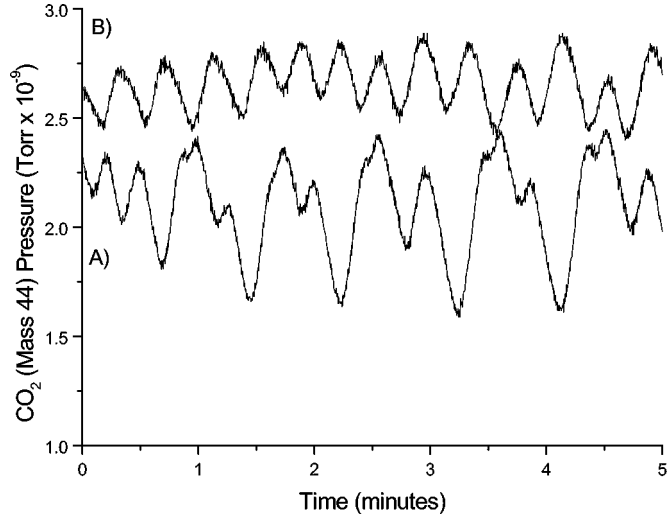

FIG. 16. Comparison of the oscillations observed on the 1.0-Pt/SiO_2–Cl catalyst with different pretreatments. Spectrum A was taken after oxidation at 300°C. Spectrum B was taken after oxidation at 450°C. Both spectra were collected at a reaction temperature of 245°C, $P = 1.2$ Torr and O_2/CO = 3.0.

simple catalyst sintering cannot explain the changes in the oscillation amplitudes. In addition, the sample of 3.0-Pt/SiO_2–NO postimpregnated with HCl displayed large amplitude oscillation if the pellet was pretreated at a low temperature (200°C). Higher temperature pretreatment (>250°C) returned the catalyst to the low-amplitude state. Therefore, the presence of chlorine impurities has a definite effect on the amplitude of oscillations and thus the size of CO islands on this series of catalysts.

3.10. The Effect of Hydrogen on Oscillatory Behavior

An additional aspect of the reaction was observed when a small amount of hydrogen was added to the feed stream. For all of the catalysts examined in this study, H_2 was shown to completely quench the oscillations and force the system into a highly reactive state. Figure 17 gives an example of this type of experiment. At point A, a pulse of H_2 was allowed to enter the feed stream. After an initial instability, the production of CO_2 is seen to stabilize at a high value (3-min mark). At point B, the flow of H_2 was shut off and the oscillations resumed. IR spectra taken during this experiment either show a very low coverage of CO on the surface with a lower frequency than has been observed during the oscillations or show no CO on the surface at all. It should also be noted that only a very small flow of H_2 (1–2 %) was necessary to quench the oscillation. The leak rate across the H_2 mass flow controller was sufficient. Mass spectrometry did not detect the presence of additional reaction products, such as water, when H_2 was introduced. Even if the O_2–H_2 reaction were occurring, the effect would be a depletion of surface oxygen and an increase in the coverage of adsorbed CO, which is the exact opposite of what was observed.

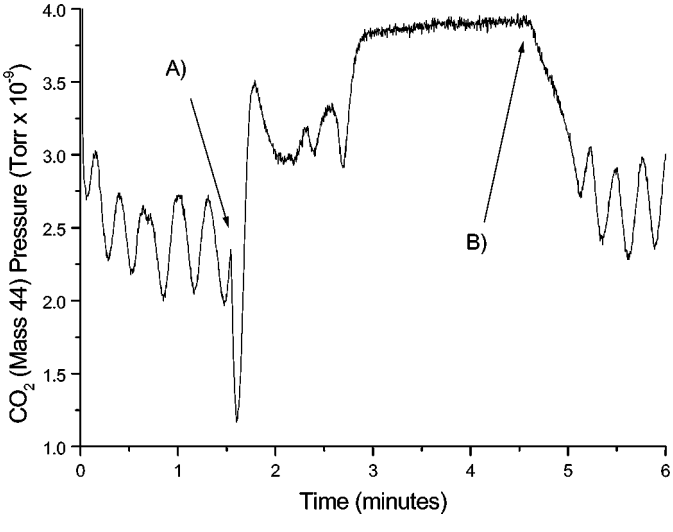

FIG. 17. Example of the effect of hydrogen on oscillatory behavior over 3.14-Pt/SiO_2–Cl. At Point A a pulse of hydrogen was allowed to enter the reactor. At point B the flow of H_2 ceased. Reaction conditions were $P = 1.3$ Torr, $T = 260$°C, and $O_2/CO = 3.0$.

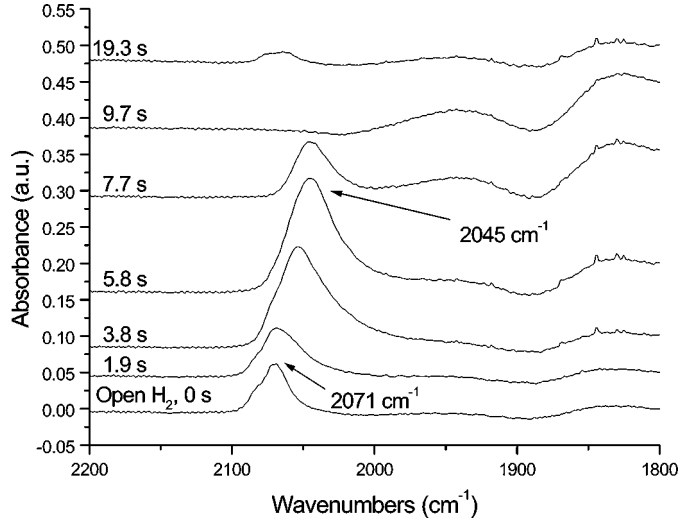

FIG. 18. FTIR spectra collected when <1% H_2 was added to reaction reactor inlet during oscillations. The sample shown is 1.0-Pt/SiO_2–Cl at 215°C and 1.2 Torr. $t = 0$ represents the introduction of H_2 into the system.

Coadsorption studies have shown that H_2 and CO form mixed islands on Pt(335) surfaces (67). Therefore, the most likely cause of this phenomenon is that H_2 molecules are small enough that they can penetrate and disperse the CO islands that exist on the surface during the reaction. This is substantiated by FTIR results obtained when H_2 is dosed onto the catalyst during oscillations, as shown in Fig. 18. At $t = 0$ s, the catalyst is in an oscillatory state and H_2 is introduced into the reactor. Within 6 s, the CO stretching frequency has red shifted 26 cm^{-1}, which based on the results of the isotope-mixing experiment implies that CO exists in a dispersed state. This claim was substantiated in a subsequent experiment (not shown) in which H_2 and CO were coadsorbed onto the catalyst surface at 240°C. The resulting CO frequency was 2042 cm^{-1}. $C^{18}O$ was then introduced into the system, which resulted in only a 1- to 2-cm^{-1} shift in the $C^{16}O$ stretching frequency, confirming the dispersed state of CO on the surface in the presence of H_2. With CO in a more dispersed state, oxygen is able to react with the entire CO layer on the surface and the catalyst immediately jumps to the highly reactive state. A similar experiment was performed with both helium and nitrogen, neither of which was able to quench the oscillations. It should also be noted that the effect of hydrogen on the oscillatory behavior cannot be explained by mass transfer limitations, providing further evidence that the oscillations are kinetic in origin.

3.11. The Driving Force for Island Formation

The evidence in this study strongly supports the existence of CO islands on the surface of the platinum that change in size during the oscillations. As mentioned in Section 1, models for the oxidation of CO that incorporate

the existence of islands have predicted oscillations (36). In that case, the nonlinearity in the differential equations occurs due to a square root dependence of the coverage of CO and oxygen in the reaction term. This dependence is consistent with the reaction occurring at the periphery of islands, but not consistent with our data. An additional mechanism has been suggested in which CO islands nucleate and grow in size until they reach a critical size (1). At this point, the adsorbed oxygen region between the CO islands becomes compressed, which changes the kinetics of that layer and provides feedback to return the system to the initial CO free state. Thus, in some cases the existence of islands on a catalyst surface is sufficient to provide the nonlinearity and/or feedback required for oscillations to occur.

The exact details of how and why the islands form in this system, however, remain unclear. In addition, the exact nature of the synergy between the islands and the oscillations remains unclear. Other forms of feedback may be contributing to the oscillations observed in this research. This system is clearly quite complicated and no single explanation appears to be appropriate. However, based on the observation made in this research, we offer the following possibilities to explain the existence of islands and oscillations in this system.

One possibility is that the presence of chlorine impurities on the platinum surface or in the bulk nucleates islands of CO. This study has shown that chlorine levels affect the amplitude of the oscillations. It is reasonable that highly electronegative chlorine atoms can interact with CO dipoles on the surface of the catalyst and stimulate the formation of close-packed CO islands. It is also reasonable that this effect would create a nonlinearity in the reaction kinetics sufficient to result in oscillations. This hypothesis may also explain why hydrogen can quench the oscillations. The presence of hydrogen on the surface of the catalyst would counteract the electrostatic effect of chlorine. However, oscillations were also observed on catalysts that were made with the chlorine-free anime–nitrate precursor. Thus, it is unlikely that chlorine is the sole driving force for the formation of islands and oscillations in this system unless the chlorine-free catalysts also contain a trace amount of chlorine (from the precursor, silica gel, or solvents used in the preparation of the catalysts.)

The second possibility is that CO island formation is the result of the surface-phase transition and micro-faceting that have been linked to oscillations and pattern formation on Pt(100) and Pt(110) single crystals (3, 7, 17, 68). Thus, the Pt(100) and Pt(110) facets on the platinum crystallites may be reconstructing in the same way that single crystals reconstruct. The islands of CO would exist on these facets during the oscillations. The change in IR peak position during the reaction does not seem to support this model. Single-crystal studies have shown that the difference in CO stretching frequency between the 1×1 and the hex phase on Pt(100) at full coverage is much greater (18 cm^{-1}) than the shift observed in this study during reaction conditions (12, 69). Conversely, it has been shown in the literature that the Pt(110) surface reconstruction is not accompanied by changes in the CO stretching frequency (70). In addition, the parameter space for oscillations over a Pt(100) single crystal has been shown to be different from that for the supported catalyst (9).

However, all of these cases considered were studies performed on single crystals under high vacuum. We have shown in this study that phenomena such as adsorbate island formation and small changes in the oxidation state of the metal can have significant effects on the IR spectrum of CO on platinum. Additionally, the existence of surface kinks, edges, and corners on the supported catalyst will alter the properties of the platinum surface and may allow a larger parameter space in which the oscillations can occur. For these reasons, not all extrapolations to the behavior of single crystals may be valid, and the Pt(100) and Pt(110) surface-phase transition remains as a possible driving force for island formation.

If the surface-phase transition is occurring on the catalysts in this system, differences in the amplitudes of the oscillations may be due to the effect of platinum particle morphology. Wang *et al.* (71) have shown that the shape of platinum particles deposited on silica substrates is highly dependent upon the pretreatment that the particles undergo. Particles treated with a high-temperature reduction were cubic in shape with mostly (100) faces. When these particles were then oxidized at a high temperature ($>450^{\circ}C$), highly faceted spherical particles with mostly (111) faces were formed. The process, however, was not reversible; further reduction did not convert the spherical crystallites back in to cubic crystallites. Shi and Masel (72) later performed surface energy calculations that supported the observations by Wang *et al.* Johansson *et al.* (73) have observed similar changes in platinum particle morphology upon the reduction and oxidation of nanofabricated model catalyst arrays.

In light of this information it is possible that the catalysts manufactured from chloroplatinic acid contain crystallites that are cubic in shape. These crystallites have large (100) facets that are able to support large continuous islands of surface CO and the surface-phase transition. The amine–nitrate catalysts, however, contain spherical, highly faceted crystallites. The small facets on the spherical particles would not be able to support large, continuous islands of CO or significantly large regions where the surface-phase transition could occur. This is consistent with the small amount of CO observed on the catalysts reaction conditions. It is also consistent with the observation that the amine samples appear to be somewhat reactive even at room temperature. If an amine–nitrate catalyst is covered with CO and then dosed with O_2, the amount of CO on the catalyst is seen to decrease rapidly. The chloroplatinic acid samples, however,

only show a small decrease in CO coverage. Since it has been shown that O_2 adsorbs more easily on corners and edges (14, 74), it stands to reason that a spherical crystallite would be more likely to be able to adsorb O_2 than would a more cubic crystallite. In this hypothesis, chlorine impurities act to stabilize the cubic shape of the crystallites. When these catalysts are heated to a high temperature in oxygen, the chlorine is removed, the particles become more rounded, and the facets become smaller. The amount of CO observed during the reaction then becomes much smaller as was observed in the experiments. However, adding chlorine to the catalyst results in the stabilization of cubic crystallites and the reappearance of large amplitude oscillations. This hypothesis is also consistent with the results of isotope-mixing experiments (Section 3.4), which suggest that the two different types of catalyst in this system may have different morphologies.

A final possible driving force for the oscillations observed in this system involves an actual change in the shape of the platinum crystallites. In this case, the distribution of facet orientations would actually be changing during the oscillations. The observed changes in the size of CO islands are then a direct result of a change in the size of the particle facet onto which the CO is chemisorbed. It has been shown in the literature that oxidizing treatment tends to create a rounded crystallite, while a reducing treatment produces a more faceted crystallite (71). In the oscillatory regime, an unstable steady state may exist between adsorbed oxygen that tends to round the particle and adsorbed CO that tends to support the growth of facets. Even though the Pt(100) or Pt(110) surface-phase transition may not have a direct role in the reshaping of the catalyst, the existence of such a change substantiates the idea that the crystallites may be able to change shape during the reaction. Clearly, the platinum atoms have some amount of mobility. It should also be noted that silica is generally considered to be a neutral support (75). Thus, the support would offer little stabilization of the metal particles that might dampen such a change in the shape of the platinum particle. Zhdanov and Kasemo (76) have performed Monte Carlo simulations that take into account changes in particle shape during a reaction. They did predict a change in the kinetic behavior of the catalyst if reshaping were allowed. They did not, however, predict any kinetic rate oscillations. Regardless of the specific feedback mechanism that is involved in this reaction, the distribution of crystallographic planes may play a role in the nature of the oscillations observed in this system.

4. SUMMARY

In this study we have employed FTIR and mass spectrometry to analyze the adsorption and desorption characteristics of a series of silica-supported platinum catalysts synthesized from a chloride-containing and a chloride-free precursor. Carbon monoxide adsorption and desorption experiments were conducted and showed a difference in the IR absorption peak shape and frequency depending upon the pretreatment given to the catalyst. These differences in the IR spectra can be directly linked to differences in platinum particle size and in the oxidation state of the platinum crystallites. Smaller platinum particles were observed to result in a lower stretching frequency for linearly bonded CO. However, CO adsorbed onto electron-deficient platinum particles was observed to result in a narrow adsorption peak at $\sim$2080 cm^{-1} regardless of particle size.

Isotope-mixing experiments were performed in order to quantify the dipole shift and chemical shift components of the coverage-dependent peak shift over each of the five catalysts. The dipole shift was found to vary linearly from 0 to 25 cm^{-1} as a function of coverage over the chloride-free catalysts. The dipole shift covered a slightly smaller range for the chloride-containing catalyst due to the presence of chlorine impurities or platinum oxide. The chemical shift was found to range from 0 to 10 cm^{-1}, rising sharply at 80% coverage for all catalyst studied. In general, the chemical and dipole shifts were found to be completely independent of platinum particle size, in contrast to the singleton frequency, which decreases with decreasing particle size.

Based on our reaction results, we have been able to rule out both the oxidation/reduction model and the carbon model to explain the oscillations in the oxidation of carbon monoxide occurring over these catalysts. We have instead found conclusive evidence suggesting that islands of densely packed CO islands exist on the catalyst surface during the oscillations. These islands of CO block a portion of the active sites and change in size during the reaction. The amplitude of the oscillations, and therefore the size of the CO islands, appears to be linked to the amount of chlorine on the platinum particles. The feedback mechanism that drives the change in island size is unclear; however, it appears to be linked to either the Pt(100) or the Pt(110) surface-phase transition, chlorine impurities, or particle reshaping during the reaction. Simulations performed based upon the dipole coupling theory predict IR stretching frequencies that are consistent with the isotope-mixing data, thermal desorption data, and the oscillation data.

ACKNOWLEDGMENTS

The authors gratefully acknowledge the Shell Research Foundation, the National Science Foundation (Grant CTS-9733821), and the GAANN Fellowship program for the support of this research. The authors also acknowledge James Basil and Tim Gross for their work in catalyst preparation and characterization.

REFERENCES

1. Böcker, D., and Wicke, E., *Ber. Bunsen-Ges. Phys. Chem.* **89**, 629 (1985).

2. Lindstrom, T. H., and Tsotsis, T. T., *Surf. Sci.* **167**, L194 (1986).
3. Eiswirth, M., and Ertl, G., *Surf. Sci.* **177**, 90 (1986).
4. Cox, M. P., Ertl, G., and Imbihl, R., *Phys. Rev. Lett.* **54**, 15,1725 (1985).
5. Lynch, D. T., Emig, G., and Wanke, S., *J. Catal.* **97**, 456 (1986).
6. Kaul, D. J., and Wolf, E. E., *J. Catal.* **91**, 216 (1985).
7. Ertl, G., *Catal. Lett.* **9**, 219 (1991).
8. Elhaderi, A. E., and Tsotsis, T. T., *ACS Symp. Ser.* **196**, 77 (1982).
9. Lauterbach, J., Bonilla, G., and Pletcher, T., *Chem. Eng. Sci.* **54**, 4501 (1999).
10. Lynch, D. T., and Wanke, S. E., *J. Catal.* **88**, 345 (1984).
11. Gorodetskii, V. V., and Drachsel, W., *Appl. Catal. A* **188**, 267 (1999).
12. Schüth, F., and Wicke, E., *Ber. Bunsen-Ges. Phys. Chem.* **93**, 191 (1989).
13. Wicke, E., Kummann, P., Keil, W., and Schiefler, J., *Ber. Bunsen-Ges. Phys. Chem.* **84**, 315 (1980).
14. Lindstrom, T. H., and Tsotsis, T. T., *Surf. Sci.* **150**, 487 (1985).
15. Lindstrom, T. H., and Tsotsis, T. T., *Surf. Sci.* **171**, 349 (1986).
16. van Neer, F., and Bliek, A., *Chem. Eng. Sci.* **54**, 4483 (1999).
17. Imbihl, R., and Ertl, G., *Chem. Rev.* **95**, 3,697 (1995).
18. Collins, N. A., Sunderesan, S., and Chabal, Y. J., *Surf. Sci.* **180**, 136 (1987).
19. Sales, B. C., Turner, J. E., and Maple, M. B., *Surf. Sci.* **114**, 381 (1982).
20. Barshad, Y., Zhou, X., and Gulari, E., *J. Catal.* **94**, 128 (1985).
21. Hartmann, N., Imbihl, R., and Vogel, W., *Catal. Lett.* **28**, 373 (1994).
22. Lund, C. D., Surko, C. M., Maple, M. B., and Yamamoto, S. Y., *Surf. Sci.* **459**, 413 (2000).
23. Cant, N. W., and Donaldson, R. A., *J. Catal.* **71**, 320 (1981).
24. Haaland, D. M., and Williams, F. L., *J. Catal.* **76**, 450 (1982).
25. Li, Y.-E., Boecker, D., and Gonzalez, R. D., *J. Catal.* **110**, 319 (1988).
26. Eischens, R. P., Francis, S. A., and Pliskin, W. A., *J. Phys. Chem.* **60**, 194 (1955).
27. Crossley, A., and King, D. A., *Surf. Sci.* **68**, 528 (1977).
28. Persson, B. N. J., and Ryberg, R., *Phys. Rev. B: Condens. Matter* **24**, 12,6954 (1981).
29. Scheffler, M., *Surf. Sci.* **81**, 562 (1979).
30. Mahan, G. D., and Lucas, A. A., *J. Chem. Phys.* **68**, 4,1344 (1978).
31. Crossley, A., and King, D. A., *Surf. Sci.* **95**, 131 (1980).
32. Shigeishi, R. A., and King, D. A., *Surf. Sci.* **75**, L397 (1978).
33. Rotermund, H. H., *Surf. Sci.* **283**, 1–3, 87 (1993).
34. Rotermund, H. H., *Surf. Sci. Rep.* **29**, 265 (1997).
35. Lauterbach, J., and Rotermund, H. H., *Surf. Sci.* **311**, 1–2, 231 (1994).
36. Mukesh, D., Morton, W., Kenney, C. N., and Cutlip, M. B., *Surf. Sci.* **138**, 237 (1984).
37. Podkolzin, S. G., Shen, J., de Pablo, J. J., and Dumesic, J. A., *J. Phys. Chem.* **104**, 4169 (2000).
38. Brandt, R. K., Hughes, M. R., Bourget, L. P., Truszkowska, K., and Greenler, R. G., *Surf. Sci.* **286**, 15 (1993).
39. Hayden, B. E., Kretzschmar, K., Bradshaw, A. M., and Greenler, R. G., *Surf. Sci.* **149**, 394 (1985).
40. Sheppard, N., and Nguyen, T. T., *in* "The Vibrational Spectra of Carbon Monoxide Chemisorbed on the Surfaces of Metal Catalysts—A Suggested Scheme of Interpretation" (R. J. H. Clark and R. E. Hester, Eds.), Vol. 5, p. 67. Heyden, London, 1978.
41. Hayden, B. E., and Bradshaw, A. M., *Surf. Sci.* **125**, 787 (1983).
42. Barth, R., Pitchai, R., Anderson, R. L., and Verykios, X. E., *J. Catal.* **116**, 61 (1989).
43. De La Cruz, C., and Sheppard, N., *Spectrochim. Acta* **50A**, 2,271 (1993).
44. Greenler, R. G., Burch, K. D., Kretzschmar, K., Klauser, R., Bradshaw, A. M., and Hayden, B. E., *Surf. Sci.* **152/153**, 338 (1985).
45. de Ménorval, L.-C., Chaqroune, A., Coq, B., and Figueras, F., *J. Chem. Soc., Faraday Trans.* **93**, 20,3715 (1997).
46. Blyholder, G., *J. Phys. Chem.* **68**, 2773 (1964).
47. Kappers, M. J., and van der Maas, J. H., *Catal. Lett.* **10**, 365 (1991).
48. Slinko, M. M., and Jaeger, N. I., "Oscillating Heterogeneous Catalytic Systems." Elsevier, New York, 1994.
49. Yamamoto, T., Shido, T., Inagaki, S., Fukushima, Y., and Ichikawa, M., *J. Phys. Chem. B* **102**, 20,3866 (1998).
50. Herz, R., and Shinouskis, E. J., *Appl. Surf. Sci.* **19**, 373 (1984).
51. Sárkány, J., Bartók, M., and Gonzalez, R. D., *J. Catal.* **81**, 347 (1983).
52. Bartók, M., Sárkány, J., and Sitkei, A., *J. Catal.* **72**, 236 (1981).
53. Araya, P., Porod, W., and Wolf, E. E., *Surf. Sci.* **230**, 245 (1990).
54. Tüshaus, M., Schweizer, E., Hollins, P., and Bradshaw, A. M., *J. Electron. Spectrosc. Relat. Phenom.* **44**, 305 (1987).
55. Hollins, P., and Pritchard, J., *Prog. Surf. Sci.* **19**, 4,275 (1985).
56. Lauterbach, J., Boyle, R. W., Schick, M., Mitchell, W. J., Meng, B., and Weinberg, W. H., *Surf. Sci.* **350**, 1–3, 32 (1996).
57. Hollins, P., *Surf. Sci. Rep.* **16**, 51 (1992).
58. Jakob, P., and Persson, B. N. J., *Phys. Rev. B: Condens. Matter* **56**, 16,10644 (1997).
59. Niemantsverdriet, J. W., "Spectroscopy in Catalysis." VCH, Weinheim/New York, 1995.
60. Stoop, F., Toolenaar, F. J. C. M., and Ponec, V., *J. Catal.* **73**, 50 (1982).
61. Fox, S. G., Browne, V. M., and Hollins, P., *J. Electron. Spectrosc. Relat. Phenom.* **54/55**, 749 (1990).
62. Welch, P. C., Mills, P. S. W., Mason, C., and Hollins, P., *J. Electron. Spectrosc. Relat. Phenom.* **64/65**, 151 (1993).
63. Bourane, A., Dulaurent, O., and Bianchi, D., *J. Catal.* **195**, 406 (2000).
64. Greenler, R. G., Leibsle, F. M., and Sorbello, R. S., *Phys. Rev. B: Condens. Matter* **32**, 12,8431 (1985).
65. Anderson, J. A., Chong, F. K., and Rochester, C. H., *J. Mol. Catal. A: Chem.* **140**, 65 (1999).
66. Fuchs, S., Hahn, T., and Lintz, H.-G., *Chem. Eng. Process.* **33**, 363 (1994).
67. Kahlich, M. J., Gasteiger, H. A., and Behm, R. J., *J. Catal.* **171**, 93 (1997).
68. Ladas, S., Imbihl, R., and Ertl, G., *Surf. Sci.* **198**, 42 (1988).
69. Gardner, P., Martin, R., Tüshaus, M., and Bradshaw, A. M., *J. Electron. Spectrosc. Relat. Phenom.* **54/55**, 619 (1990).
70. Imbihl, R., Behm, R. J., Christmann, K., Ertl, G., and Matsushima, T., *Surf. Sci.* **117**, 257 (1982).
71. Wang, T., Lee, C., and Schmidt, L. D., *Surf. Sci.* **163**, 181 (1985).
72. Shi, A. C., and Masel, R. I., *J. Catal.* **120**, 421 (1989).
73. Johansson, S., Wong, K., Zhdanov, P., and Kasemo, B., *J. Vac. Sci. Technol., A* **17**, 1,297 (1999).
74. Sárkány, J., and Gonzalez, R. D., *Appl. Catal.* **5**, 85 (1983).
75. Stakheev, A. Y., and Kustov, L. M., *Appl. Catal., A* **188**, 3 (1999).
76. Zhdanov, V. P., and Kasemo, B., *Phys. Rev. Lett.* **81**, 12,2482 (1998).